Marroquin, Jason B., Harold A. Coleman, Mary A. Tonta, Kun Zhou, Bjorn Winther-Jensen, James Fallon, Noel W. Duffy, Edwin Yan, Ammar A. Abdulwahid, Jacek J. Jasieniak, John S. Forsythe, and Helena C. Parkington. 2017. Neural Electrodes Based on 3D Organic Electroactive Microfibers. *Advanced Functional Materials*: 1700927.

doi: 10.1002/adfm.201700927

Advanced Functional Materials

Neural electrodes based on 3-dimensional organic electroactive microfibers

--Manuscript Draft--

Manuscript Number:	adfm.201700927R1
Full Title:	Neural electrodes based on 3-dimensional organic electroactive microfibers
Article Type:	Invited Full Paper
Keywords:	neural electrodes; neural interface; PEDOT; electrophysiology
Corresponding Author:	John Forsythe, Prof. Monash University Melbourne, AUSTRALIA
Corresponding Author Secondary Information:	
Corresponding Author's Institution:	Monash University
Corresponding Author's Secondary Institution:	
First Author:	Jason Marroquin Reyes, BSc
First Author Secondary Information:	
Order of Authors:	Jason Marroquin Reyes, BSc
	Harold A Coleman, PhD
	Mary A Tonta, BSc
	Kun Zhou, PhD
	Bjorn Winther-Jensen, PhD
	James Fallon, PhD
	Noel W Duffy, PhD
	Edwin Yan, PhD
	Ammar Abdulwahid
	Jacek J Jasieniak, PhD
	John Forsythe, Prof.
	Helena C Parkington, PhD
Order of Authors Secondary Information:	
Abstract:	Neural electrodes used for in vivo biomedical applications (e.g. prostheses, bionic implants) result in glial invasion leading to the formation of a non-excitable scar which increases the distance between neurons and electrode and increases the resistance to current flow. The result is progressive deterioration in the performance of stimulation or recording of neural activity and inevitable device failure. Also, electrodes with a 2-dimenstional (2D) surface have a limited proximity to neurons. In the present study, a macroporous and fibrous 3-dimensional (3D) neural electrode was developed using poly-L-lactic acid fibrous membranes imbued with electroactive properties via a coating of the conductive polymer poly(3,4-ethylenedioxythiophene) (PEDOT), using vapor phase polymerization. The electrical properties of the PEDOT coated substrates were studied using sheet resistance and impedance. PEDOT electrode biocompatibility was assessed through in vitro assays using patch clamp electrophysiology and calcium imaging of isolated and cultured rat hippocampal neurons. PEDOT fibers supported robust normal functional development of neurons, including synaptic networking and communication. Stimulation and recording of activity in brain slices, and from the surface of the brain using 3D-PEDOT fibrous electrodes were indistinguishable from recordings using conventional glass or platinum electrodes. In vivo studies revealed

	minimal reactive gliosis in response to electrode implantation.

Neural electrodes based on 3-dimensional organic electroactive microfibers

[1,2]Jason Marroquin Reyes, [1]Harold A. Coleman, [1]Mary A. Tonta, [2]Kun Zhou, [3]Bjorn Winther-Jensen, [4]James Fallon, [5]Noel W. Duffy, [1]Edwin Yan, [1,6]Ammar Abdulwahid, [7]Jacek J. Jasieniak, [2]John S. Forsythe, [1]Helena C. Parkington**

[1]Department of Physiology, Biomedicine Discovery Institute, Monash University;
[2]Department of Materials Science and Engineering, Monash Institute of Medical Engineering, Monash University;
[3]Department of Advanced Science and Engineering, Waseda University, Tokyo 169-8555, Japan;
[4]The Bionics Institute, East Melbourne, Australia;
[5]CSIRO Energy Flagship, Ian Wark Laboratories, Bayview Ave, Clayton, Victoria 3168, Australia;
[6]Department of Physiology and Pharmacology, College of Veterinary medicine, University of Baghdad, Baghdad, Iraq.
[7]Department of Materials Science and Engineering, Monash Energy Materials and Systems Institute.
*co-corresponding authors

ABSTRACT

Neural electrodes used for in vivo biomedical applications (e.g. prostheses, bionic implants) result in glial invasion leading to the formation of a non-excitable scar which increases the distance between neurons and electrode and increases the resistance to current flow. The result is progressive deterioration in the performance of stimulation or recording of neural activity and inevitable device failure. Also, electrodes with a 2-dimenstional (2D) surface have a limited proximity to neurons. In the present study, a macroporous and fibrous 3-dimensional (3D) neural electrode was developed using poly-L-lactic acid fibrous membranes imbued with electroactive properties via a coating of the conductive polymer poly(3,4-ethylenedioxythiophene) (PEDOT), using vapor phase polymerization. The electrical properties of the PEDOT coated substrates were studied using sheet resistance and impedance. PEDOT electrode biocompatibility was assessed through in vitro assays using patch clamp electrophysiology and calcium imaging of isolated and cultured rat hippocampal neurons. PEDOT fibers supported robust normal functional development of neurons, including synaptic networking and communication. Stimulation and recording of activity in brain slices, and from the surface of the brain using 3D-PEDOT fibrous electrodes were indistinguishable from recordings using conventional glass or platinum electrodes. In vivo studies revealed minimal reactive gliosis in response to electrode implantation.

1. Introduction

Neural electrodes need to meet a broad spectrum of criteria dictated by the desired application.[1-2] Since success depends on an appropriate and maintained interface between neurons and the stimulating and/or recording electrodes, it is crucial to consider the material as well as the conformation to be used for electrode fabrication[3]. Neural electrodes have typically been fabricated in different conformations, such as microwires and microfabricated electrode arrays, mostly using stiff materials such as silicon, platinum, gold, diverse metallic alloys and iridium oxide.[2, 4] Although these types of electrodes have long been used, mechanical mismatch between the stiff electrode and soft neural tissue causes shear-induced inflammation. This inflammation results in the formation of a glial scar which, over time, encapsulates and isolates the electrode from the target neural tissue.[4-5] Hence, management of electrode stiffness is critical for long term implant stability.[6]

Several approaches have been proposed to reduce the undesirable inflammatory reactive responses to implanted electrodes. These approaches have included reducing device size[7] and modification of device surface. Such modifications have included roughening[8], adding a biocompatible coating,[5, 8-9] modulating stiffness,[10] or functionalizing with adhesion/trophic factors and anti-inflammatory agents.[4-5, 7-13]

The mechanical properties of conducting polymers are significantly different from semiconductors and metals.[10] As a result of their reduced stiffness, they have been widely used as soft electronics for biosensor and biomedical applications [14]. Among conductive polymers, poly (3, 4-ethylenedioxythiophene) (PEDOT) has desirable properties required for neural interfaces such as low resistivity, good stability and compatibility with biological tissues.[15-18] Also, the active surface area of PEDOT coatings can be increased further through swelling into porous hydrogel electrodes.[19] In addition, PEDOT can be doped with different anions, selected according to the properties they impart, and thus provide optimal features for implanted electrodes.[20] The use of polystyrene sulphonate (PSS) as a counter ion is well established while working with organic electronics. However, the use of tosylate (TOS) allows for *in situ* vapor phase polymerization (VPP) that produces well-adhering, highly conducting and ordered thin films on different substrate morphologies and the facile incorporation of other molecules without hindering its electrical and physical properties.[21-26]

Although PEDOT has been widely used in neural devices, these have been effectively two-dimensional (2D). This geometric arrangement provides limited accessibility to neurons and needs to be taken into account when fabricating an electrode. Developments in tissue engineering have attempted to construct electrodes that more closely mimic the *in vivo* 3-dimensional (3D) environment, both in morphology and function via 3D micro/nano fabrication techniques.[27-29] Other approaches to minimize the electrode footprint in neural tissue have included PEDOT coating of the tips of micron diameter carbon fibers[30] and self-unfolding silicon nanowire mesh electronics,[31] suggesting that a 3D porous interface allows enhanced neural interactions.

Electrospinning has been widely used in engineering devices for neural tissue applications due to its versatility in the type of biomaterials, as well as control over the physical and mechanical dimensions of the products.[32-34] Only a limited number of studies have combined conductive polymers with electrospun fibers for electrode fabrication. Nanofiber templates have been electrochemically coated with PEDOT on the surface of "Michigan" neural microelectrodes with iridium recording sites.[35] The PEDOT nanotubes

presented lower impedance and higher charge capacity density compared with a simple film coating. Another study applied PEDOT coatings on nanofibers to electrically induce Ca^{2+} signaling in SH-SY5Y neuroblastoma cells *in vitro*,[36] but were only assessed for up to 48hr.

In the present study microfibrous electrodes were fabricated using electrospun poly-L-lactic acid (PLLA) templates, which we have used previously.[37] These were then coated with PEDOT. Acutely isolated hippocampal neurons were seeded onto these microfibrous membrane electrodes. Neuron function was tested in terms of network formation using patch-clamp electrophysiology and calcium imaging over a period of 42 days. Electrical activity was recorded from and induced in brain slices in a manner that was indistinguishable from glass electrodes. Microfiber membrane electrodes placed on the brains of anesthetized guinea-pigs also recorded activity that was indistinguishable from that recorded via platinum electrodes. Platinum electrodes notoriously induce scarring.[5] However, prolonged contact of our mats on the brains of free-running rats for three weeks did not induce scarring. Hence we address three important issues: (1) fabrication of a fully functional electrode interface that; (2) sustains neural development and; (3) most importantly, is a new flexible interface that does not induce a negative inflammatory response. Concordantly, we hypothesize that these membranes electrodes will sustain neural development, providing microcellular environment to support intimate electrical contacts between neurons resulting in reliable long-term neural electrodes.

2. Results and Discussion

The following results outline the use of three different types of PEDOT conformations: 2D-PEDOT (flat 2D substrate) was used to test just the biocompatibility of PEDOT. Fiber monolayer coated with PEDOT (FM-PEDOT) facilitated biocompatibility patch-clamp recordings in a PEDOT fibrous environment, since technical difficulties preclude such recordings from 3D-PEDOT. 3D-PEDOT (fibrous mats coated with PEDOT) were the structures of primary interest. Calcium imaging of cells on FM-PEDOT provided overlap in biocompatibility testing with calcium imaging on 3D-PEDOT. Finally, the functional capability of 3D-PEDOT mats was tested *in vitro* in brain slices and *in situ*.

2.1. Characterization of electrospun microfibers

The morphology of the fibers was characterized using scanning electron microscopy (SEM). Electrospun PLLA formed a fibrous membrane with evenly distributed fibers in a random woven structure and a median fiber diameter of 1.0 µm (IQR= 0.3) (**Figure S.1**). This fiber structure was maintained when the vapor phase polymerization (VPP) of PEDOT was applied; PEDOT covered the fibers resulting in a rougher surface and an increased median fiber diameter of 1.4 µm (IQR= 0.2) (**Figure 1a**), but the 3D porous structure of the membrane was preserved (**Figure 1b & S1c**).

To determine the electrical properties, the sheet resistance of VPP-coated fibrous membranes was measured by 4-point probe analysis. Results in **Figure 1c** show that 2D-PEDOT had the lowest sheet resistance, compared with the PLLA fiber monolayer samples coated with PEDOT (FM-PEDOT) or PLLA fibrous mats coated with PEDOT (3D-PEDOT). These results are in agreement with the sheet resistance values obtained in previous studies with

similar PEDOT thickness using the same VPP protocol on non-conductive 2D[26] and 3D[25] substrates.

Cyclic voltammograms (CVs) show (**Figure S.2**) that the signature of PEDOT redox-behavior is independent of morphology, demonstrating it is the same quality of PEDOT on all samples, i.e. the shapes of the CVs are similar for all samples when diffusion phenomena were minimized using a low scan rate (5mV/s). The data also show that the redox capacity of PEDOT, and thus the amount of PEDOT for the samples, is different when going from 2D to a 3D geometry. Calculating the charge by integrating the area of each respective cycle results in a ratio of 1:8:27 for 2D-PEDOT: FM-PEDOT: 3D-PEDOT, respectively. This is an expected result since a 3D substrate has a higher surface area with a concomitant larger amount of PEDOT needed to cover such a surface. Additionally, the gradual distortion of the CVs when going from 2D to 3D substrates is apparently caused by a higher resistance combined with a much higher redox capacity. Since the measured sheet resistances values were similar (**Figure 1c**) for all PEDOT substrates, this means that the additional PEDOT in the 3D samples compensates for the hindered geometry for conduction, i.e. longer conduction pathway. This appears as a delayed effect of the redox system and a tilt in the CVs shape, because the resistance per PEDOT unit over the measured area is higher than for a 2D sample. Hence, it is "more difficult" to get charge through to each PEDOT unit in the 3D samples, this is further evinced in the increased impedance for 3D samples (**Figure 1d**).

The redox couple at ~0.2V (reduction) and ~0.4V (oxidation) seen in FM-PEDOT and 3D-PEDOT is from trapped/coordinated iron (Fe) from the Fe(III) TOS oxidant and the redox shifting is between Fe(II) and Fe(III). The Fe is very likely coordinated with the PLLA substrate, i.e. the ester groups.[38] This Fe system does not influence the PEDOT redox-system, since PEDOT is just acting as an electrical connection, facilitating the charge-transfer to the Fe (II)/Fe (III) system.[21, 39] This effect is, to a lesser extent, expressed in 2D-PEDOT as the redox couple at 0.05/0.25V. As discussed in further detail later in the electrophysiology results, we believe the presence of Fe and its redox couple do not have any effect on the function of PEDOT as a substrate for the cells or for the communication with the cells, since Fe will not be on the surface of PEDOT, but attached to the PLLA substrate.

Figure 1d &1e shows electrochemical impedance spectroscopy of PEDOT coated substrates. The Bode plot shows that all substrates were capacitive in the low frequency range (<10Hz), with their phase angle dramatically decreasing in the 1-100Hz frequency range (**Figure 1e**). Additionally, all substrates exhibited a more resistive phase angle at 1 kHz, with lower impedance modulus (|Z|) of 110±6 Ohm (Ω) for 2D PEDOT, 216±11 Ω for FM-PEDOT and 345±6 Ω for 3D-PEDOT; this signature of impedance behavior has been observed for other PEDOT substrates.[9, 40] Results for PLLA fiber samples without a PEDOT coating were non-conductive and are not shown. The mean PEDOT coating thickness on a 2D-PLLA surface was 0.50 ± 0.02 µm as determined by optical profilometry. Additionally, the relative resistance upon flexure was determined (**Figure S.3**) to test the robustness of the electrical properties on all PEDOT samples.[41] These results showed a gradual increase in resistance with progressing bend testing. The FM-PEDOT samples had the largest resistance gain, by nearly doubling over 150 bend cycles. In contrast, 3D-PEDOT samples showed only a 40 % increase over 200 bend cycles. The 2D-PEDOT sample was much more stable because it is supported by a 1mm thick PLLA film compared to the micron sized fibers supporting 3D-PEDOT. The highest resistance stability of 3D-PEDOT compared to FM-PEDOT is explained by the relatively higher amounts of PEDOT in 3D substrates as determined by

CVs.

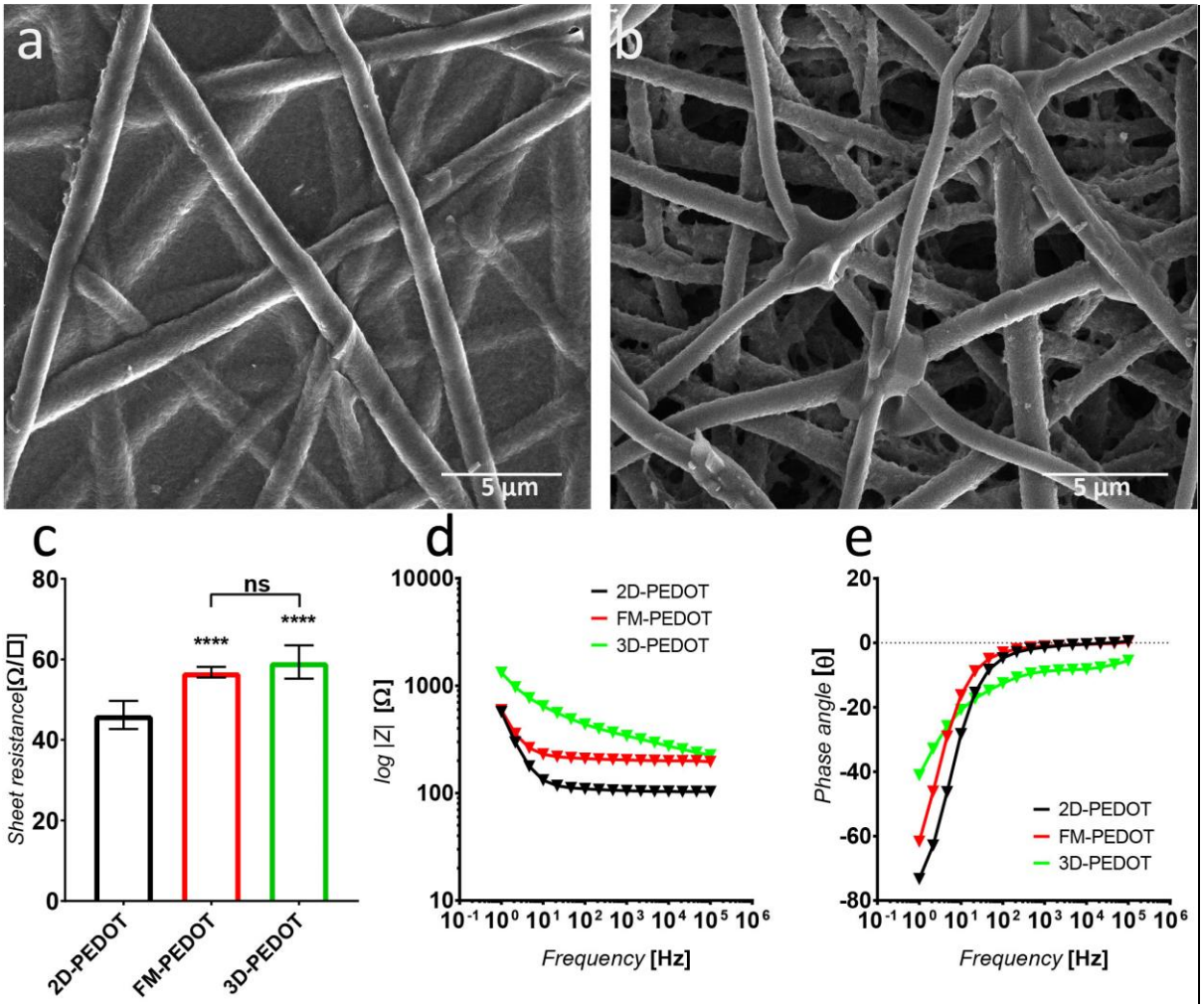

Figure 1. Scanning electron microscopy (SEM) images of **a)** FM-PEDOT and **b)** 3D-PEDOT. Electrical properties of PEDOT coated substrates: **c)** Sheet resistance (n = 10); p <0.0001 (****) 2D-PEDOT versus PEDOT fibres; no significant difference between fibre types (ns). Standard deviation is represented by error bars. **d)** Bode magnitude plot and **e)** phase plot of electrochemical impedance spectroscopy over a frequency range of 1 – 100000 Hz.

2.2. Neuron function on PEDOT: electrophysiology

Neurons are excitable cells that process and transmit information using electricity and the processes involved are best studied using electrophysiological recording approaches, including patch clamp. Large, fast changes in membrane potential, action potentials (APs), form the basis of neural function. Information transfer between neurons, networking, is achieved by AP-induced release of chemical neurotransmitter at the synapse of one neuron which may lead to the generation of an AP in the post-synaptic neuron, all of which can be recorded electrophysiologically. The ability of acutely isolated hippocampal neurons to develop and function on PEDOT substrates was studied using patch clamp electrophysiology

(**Figure 2a**) to interrogate a battery of electrophysiological properties[42] (**Figure 2b**).

Patch clamp experiments, in free-running voltage mode, revealed that neurons cultured on 2D-PEDOT and FM-PEDOT had similar characteristics to neurons growing on conventional glass, all coated with poly-L-ornithine and laminin (ANOVA, p>0.05, **Figure 2**). Across all substrates, resting membrane potential was more negative at early days *in vitro* (DIV) and became progressively less negative with time, to stabilize by 14 DIV (ANOVA, p=0.0004, **Figure 2b**). This indicates the presence of a dominant potassium conductance early in culture, with the maturation of additional ion channels with time.[43] In voltage clamp mode, a robust voltage gated sodium current, evoked using depolarizing voltage steps, increased in amplitude and speed with time and was fully established by 14 DIV and, as a consequence, in free-running voltage mode, the APs were large and brisk by this time (**Figure 2b**), indicating an increase in the density of voltage-gated sodium channels. The role of voltage-gated sodium currents in the APs was confirmed by the abolition of all APs by tetrodotoxin (**Figure 3b**), a well-established selective blocker of these ion channels. Similarly, other variables, membrane time constant, threshold for the initiation of an AP, and AP peak amplitude and maximum rates of rise and fall, were not different in neurons cultured on PEDOT compared with on glass (data not shown). It is evident from **Figure 2** that neuron maturation and characteristics were similar and occurred at the same rate when cultured on PEDOT or glass, both covered with poly-L-ornithine and laminin.

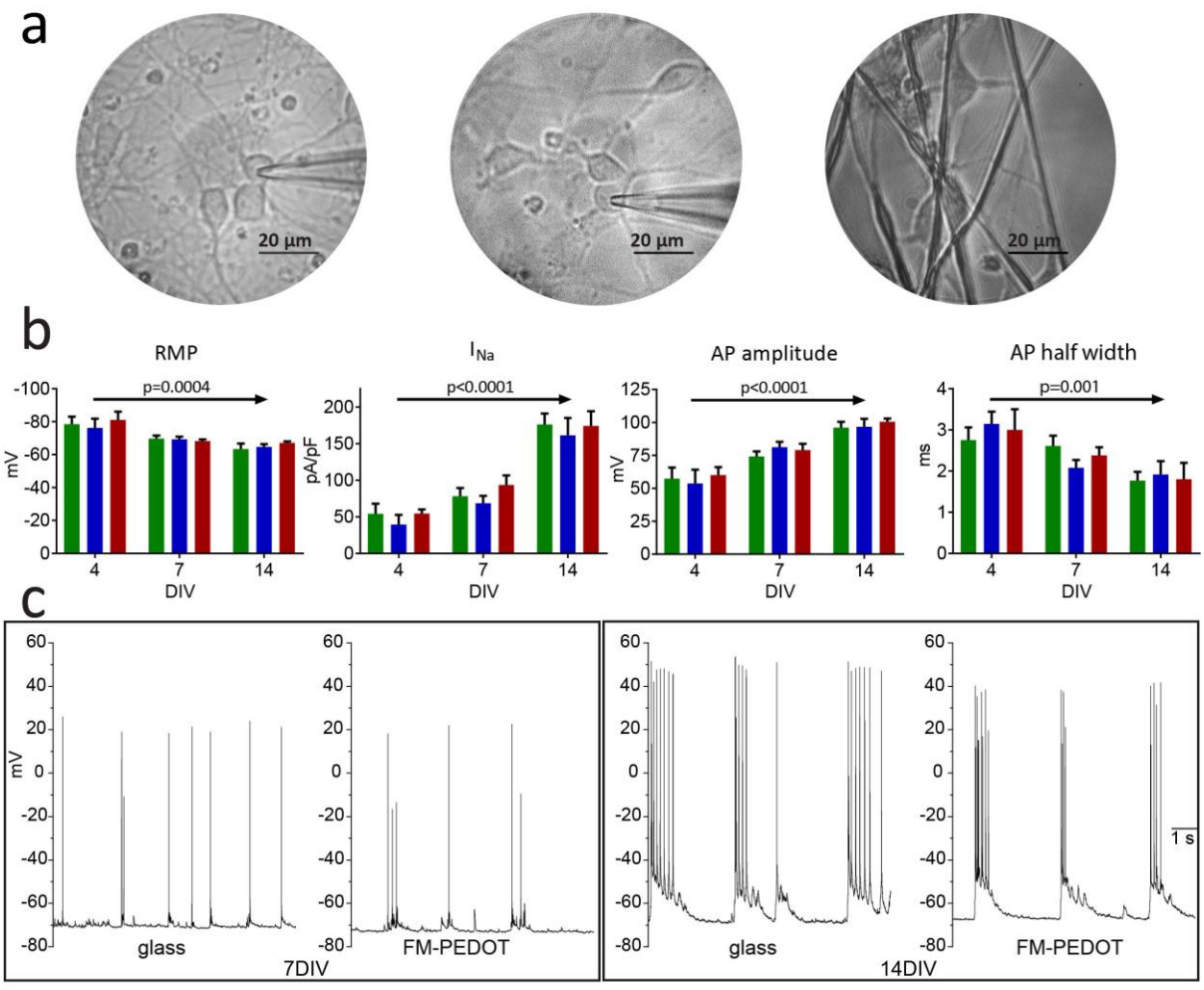

Figure 2. a) Hippocampal neurons cultured on glass (left), 2D-PEDOT (center) and FM-PEDOT. **b)** Resting membrane potential (RMP), sodium current (I_{Na}), action potential (AP) amplitude and half-width in neurons on glass control (green), 2D-PEDOT (blue) and FM-PEDOT (red) substrates at 4 DIV (cells from 8 different rats (n=8), 7 DIV (n=9) and 14 DIV (n=7) days in culture. **c)** Spontaneous networking activity developed as early as 7 DIV (left 2 panels, glass and FM-PEDOT) and increased with time (right 2 panels glass and FM-PEDOT at 14 DIV).

By 4 DIV, excitatory post-synaptic potentials (EPSPs) occurred spontaneously, and some EPSPs were sufficiently large to reach threshold for the initiation of APs. With increasing time in culture the frequency of spontaneous EPSPs and APs increased to plateau at around 14 DIV (14 DIV in **Figure 2c,** right-hand panels). EPSPs occur as a consequence of chemical neurotransmitter release from a synaptic terminal and its interaction with receptors on the receiving neuron at a synapse. When multiple EPSPs occur in short time periods they overlap, and the additive effect on membrane depolarization leads to the membrane potential reaching threshold for the initiation of an AP (**Figure 2c**). This demonstrates the normal development of synapses and functional inter-neuronal network communication on PEDOT.

At an early stage (7 DIV) and in current clamp mode (with voltage free to change, as occurs *in vivo*), normal neuron diversity was evident on 2D- and FM-PEDOT (**Figure S4**). In brief, neurons that fire a sustained volley of APs during the entire duration of a depolarization are called tonic, while those that display transient firing of 1-2 APs only at the onset of a depolarizing stimulus are called phasic. Whether a neuron is tonic or phasic is determined by its repertoire of ion channels and the presence or absence of gap junction connections with other neurons.[44] The tonic or phasic nature of a neuron has a major impact on its role in networking between neurons. Both tonic (**Figure S4a & b**) and phasic (**Figure S4c & d**) neurons were supported by PEDOT in a manner that was indistinguishable from neurons cultured on glass (data not shown). In addition, and also similar to observations on glass, some neurons on PEDOT possessed after-depolarization (**Figure S4e**) or after-hyperpolarization (**Figure S4f**) upon removal of the depolarizing current step. Thus, PEDOT supported neuron types possessing a wide variety of ion channels and signaling systems.

Normal neural networking requires the presence of both excitatory (accelerator) and inhibitory (a brake) neurons and imbalances can give rise to disease, for instance, the over-excitability of epilepsy. Thus, we further tested whether PEDOT might favor neuron types at the level of their excitatory or inhibitory neurotransmitter properties. The persistence of both excitatory (calmodulin kinase II, red staining) and inhibitory neurons (glutamic acid decarboxylase, green staining) was evident in neuronal populations cultured on glass, 2D-PEDOT and FM-PEDOT **(Figure 3a)**. This was tested functionally using activators of excitatory receptors, via a mixture of the major brain excitatory neurotransmitters glutamate and glycine, and also isoguavacine, an activator of a potent inhibitory receptor in brain, γ-

aminobutyric acid (GABA). Application of these agents demonstrated the presence of both excitatory and inhibitory neurons cultured on glass control, 2D-PEDOT and FM-PEDOT (**Figure 3b**). Therefore, it is apparent that PEDOT supports the full range of neuronal types, which is important for its use as an electrode device.

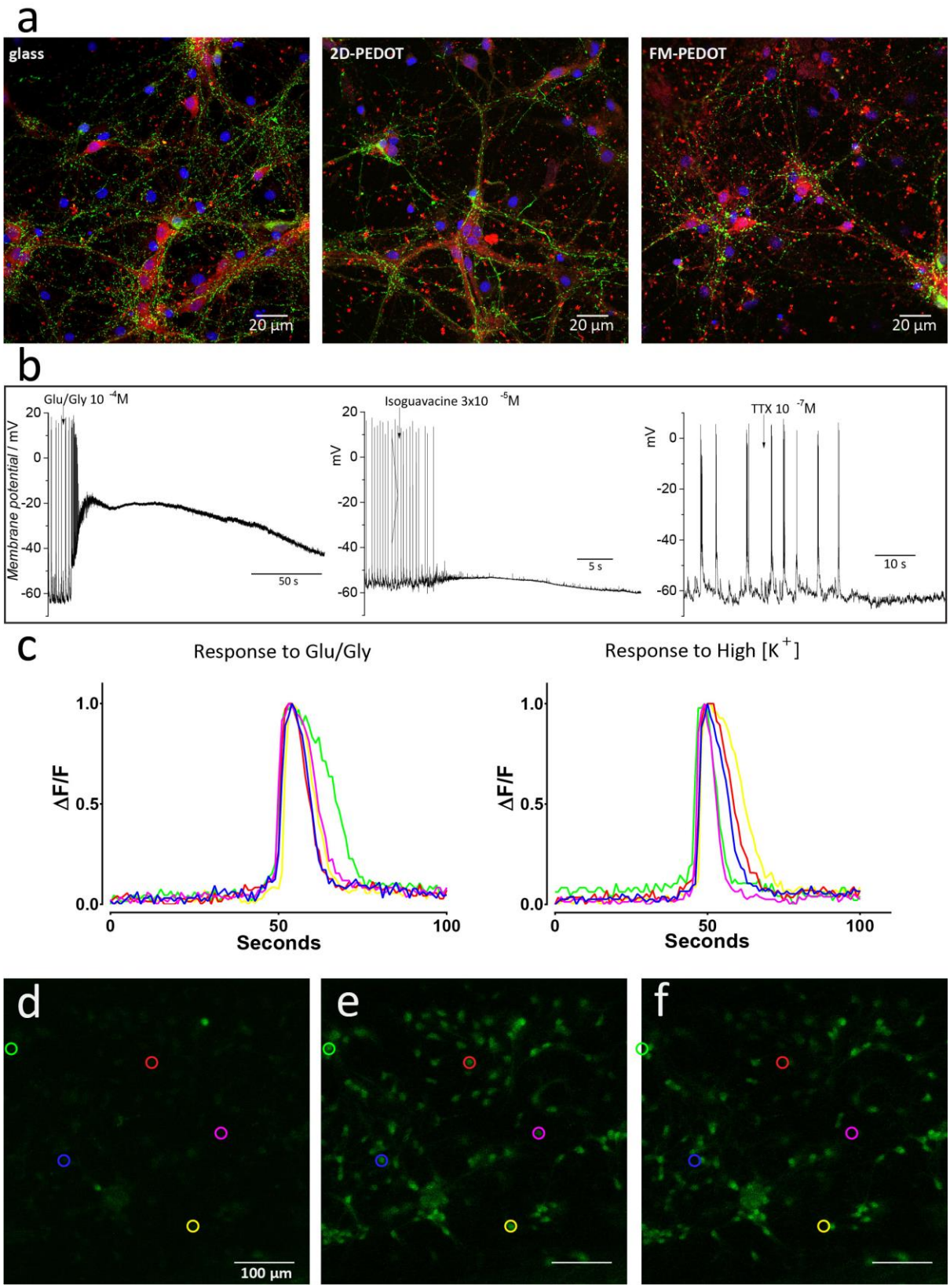

Figure 3. a) Excitatory neurons (14 DIV), as indicated by calmodulin kinase II staining of cell bodies in red, and inhibitory neurons, as indicated by glutamic acid decarboxylase staining of nerve terminals in green, (with blue DAPI staining of nuclei) in neurons cultured on glass (left), 2D PEDOT (center) and FM-PEDOT (right). **b)** Some neurons depolarized markedly in response to a 10 s application of the excitatory neurotransmitter mixture, glutamate plus glycine (n=7 cultures). Spontaneous activity ceased in other neurons upon application of the inhibitory receptor agonist, isoguavacine (n=8 cultures). Activity in most neurons was abolished by tetrodotoxin (TTX, n=8 cultures) which blocks voltage-gated sodium channels and hence APs. Cytoplasmic calcium levels in cultured hippocampal neurons at 15 DIV. **c)** Normalized fluorescence changes in cytoplasmic calcium in response to high-K solution (HiK-PSS) and to excitatory neurotransmitters glutamate plus glycine in cultures on glass. Snapshots of fluorescence images **d)** before applying HiK-PSS and at highest intensity following application of **e)** HiK-PSS and **f)** Glu/Gly.

2.3. Neuron function on 3D-PEDOT: calcium imaging

To evaluate the biocompatibility of PEDOT electrodes for extended periods of time, neural activity was assessed using fluorescence calcium imaging. Calcium imaging permits functional testing over longer time periods than are possible with electrophysiology. The reason for this is that, with time, neurons, astrocytes and microglia, secrete an extracellular matrix, a specialized perineuronal net, which is important for synaptic development and inter-neuronal networking.[45] This net can impede the formation of the intimate seal between a patch electrode and the neuron membrane, critical for patch clamp measurements. During neural activity, free cytoplasmic calcium increases to support neurotransmitter release, signaling, and synaptic maintenance and growth, and measurements of this variable can be achieved over long periods of time irrespective of the presence of the extracellular matrix. Hippocampal neurons were cultured on glass coverslip controls and on 3D-PEDOT and images were acquired twice weekly for up to 42 DIV. Neurons were selected as regions of interest (ROIs) and function was evaluated as relative changes in fluorescence intensity ($\Delta F/F$) corresponding to increases in intracellular free calcium from baseline. ROIs are presented in different colors (red, blue, green, yellow and pink) for different cells in the field of view. **Figure 4(f, K & i)** clearly shows transient increases in fluorescence intensity with time in different neurons at 42 DIV, indicating spontaneous networking.

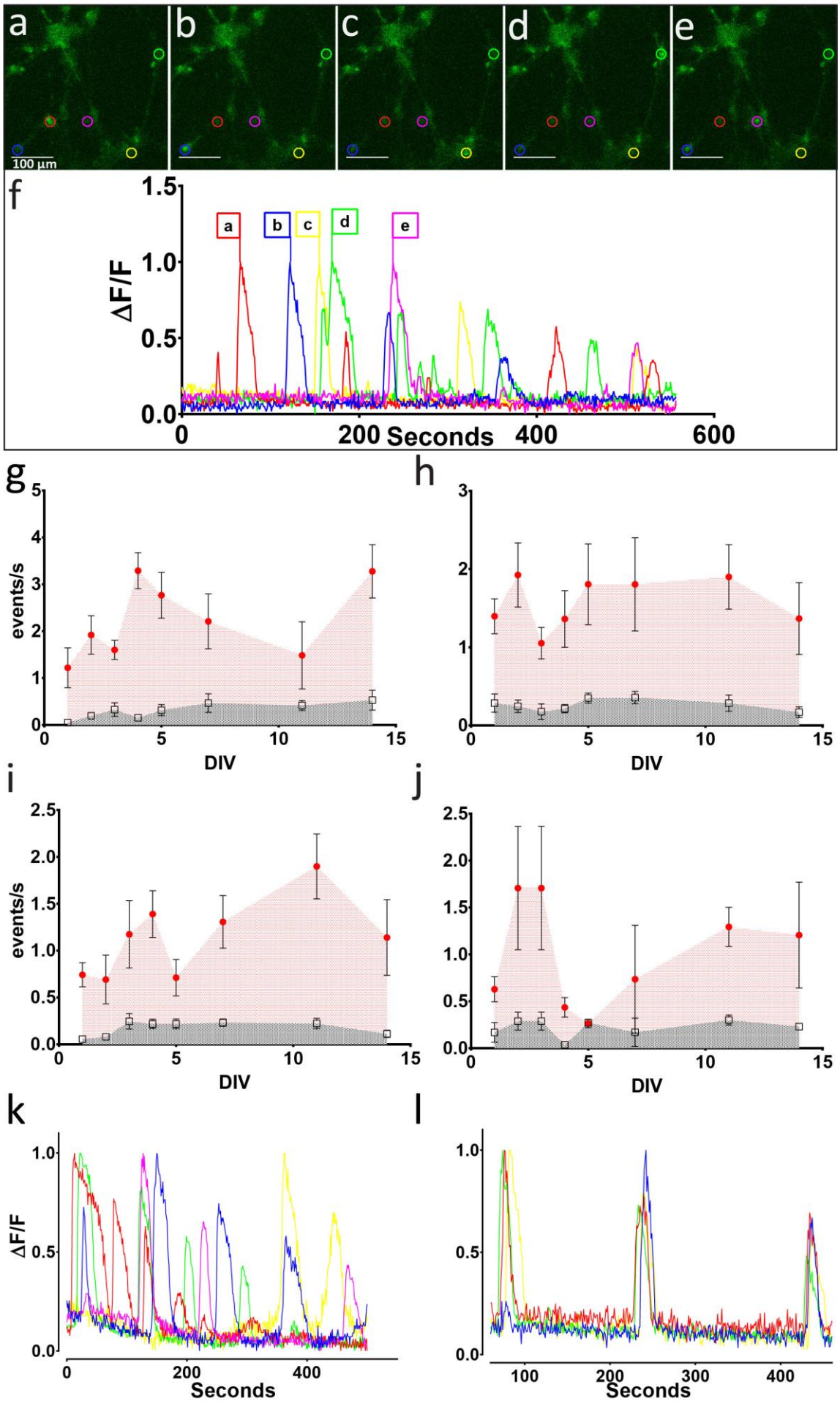
a
b
c
d
e
100 µm
f
ΔF/F
1.5
1.0
0.5
0.0
a
b
c
d
e
0
200
Seconds
400
600
g
events/s
DIV
h
DIV
i
events/s
DIV
j
DIV
k
ΔF/F
Seconds
l
Seconds

Figure 4. Spontaneous increases in cytoplasmic free calcium in hippocampal neurons cultured on 3D-PEDOT at 42 DIV. Sequential snapshots **(a-e)** of a selection of neurons (red, blue, yellow, green and pink), summarized in **f)**. The frequency of spontaneous calcium transients (mean ± SEM, cultures from 6 rats) occurring before and after addition of high K^+ and Glu/Gly at 1-14 DIV. Open squares (□) before high K^+-Glu/Gly. Red circles (●) after high K^+-Glu/Gly. Calcium transient events on **g)** glass, **h)** 2D-PEDOT, **i)** FM-PEDOT, and **j)** 3D-PEDOT. Spontaneous increases in cytoplasmic calcium in cultured hippocampal neurons at 42 DIV **k)** on glass and **l)** on 3D-PEDOT.

Neurons cultured on glass were exposed to high potassium-physiological saline solution (HiK-PSS) for 10 s in order to depolarize the neurons and evoke synchronized APs, which resulted in a synchronized elevation in cytoplasmic calcium and an increase in fluorescence intensity (**Figure 3c**). Responses to the excitatory neurotransmitters, glutamate plus glycine (Glu/Gly) for 10 s, were also studied, as this replicates physiological neurotransmitter release which also leads to a synchronized increase in cytoplasmic calcium (**Figure 3c**). Similarly, cells cultured on 3D-PEDOT also presented a robust response to HiK-PSS and Glu/Gly (**Figure 3d-f**). It is worthy of note that this brief application of Glu/Gly evoked a prolonged increase in cytoplasmic calcium in some neurons (green, yellow and, blue ROI in **Figure S5**). There was no observable difference in behavior between cultures on 3D-PEDOT compared with those on glass. Importantly, the presence of spontaneous and induced synchronized calcium fluxes reflects the robust nature of functional development in neurons cultured on 3D-PEDOT. These results demonstrate normal survival and intact function.

Recording cytoplasmic calcium provided strong evidence that neuron development proceeds similarly across time and culture substrate on PEDOT as it does on glass (**Figure 4 g-j**). Spontaneous calcium transients before exposure to HiK-PSS and Glu/Gly occurred at similar frequencies in neurons cultured on glass and on PEDOT. In some cultures spontaneous activity occurred all over the field of view with only partial synchrony (**Figure 4k).** However, in many cultures clusters of cells spontaneously fired calcium surges that were highly synchronized (**Figure 4l**), demonstrating sophisticated neuronal networking and supporting observations with electrophysiological recordings. Cultures were exposed to tetrodotoxin (TTX) and, similar to observations in electrophysiological studies of younger cultures (**Figure 3b**), it suppressed all calcium activity recorded on both control and PEDOT.

2.4. 3D-PEDOT used as electrodes to record from and stimulate acute specimens.

Glass electrodes are conventionally used to stimulate and record neuronal activity from cultured cells and brain slices.[46] Traditionally these electrodes are filled with artificial cerebrospinal fluid (aCSF), with connection to the amplifier via an Ag/AgCl wire electrode. Here we replaced the electrode content with fine 3D-PEDOT membranes, 100 µm in length, 400 µm in width and a thickness of 100 µm (**Figure S.6**), to stimulate and record from neurons in brain slices in the hippocampal region. Using conventional glass electrodes to stimulate the Schaffer collateral tract emanating from the hippocampal CA3 region evoked field EPSPs (fEPSPs) in the CA1 region which were recorded by conventional glass electrodes (**Figure 5a**), as expected. Replacing the stimulating electrode with a PEDOT electrode (n=18

slices, from 7 rats) evoked fEPSPs (**Figure 5a**) that were indistinguishable from those evoked by conventional glass electrodes. Similarly, replacing the recording electrode with a PEDOT electrode (n=16 slices, from 7 rats) recorded fEPSPs identical to those recorded by conventional glass electrodes (**Figure 5a**).

Acute electrophysiological experiments were also carried out to record surface local field potentials (LFPs) from guinea pig auditory cortex (**Figure 5b**). Responses recorded using 3D-PEDOT strips of different dimensions were similar to those recorded using a 1.5 mm diameter conventional platinum ball electrode. All electrodes were capable of recording large stimuli-evoked LFPs with peaks at latencies of approximately 10 ms. The signal-to-noise ratio (SNR) for each electrode was quantified by calculating the peak-to-peak response amplitude between 2 and 40 ms post stimulus compared with baseline activity. There was no significant difference in mean SNR for the different materials (one-way ANOVA; Holm-Sidak post-hoc; $p > 0.4$), but all responses were significantly ($p < 0.001$) greater than those recorded with non-conductive uncoated 3D-PLLA (Ctrl). These results demonstrate that 3D-PEDOT strips, not only support the development and sustained networking of neurons, but also function as stimulating and recording electrodes under laboratory conditions and in intact animals. Their performance is indistinguishable from that of conventional electrodes.

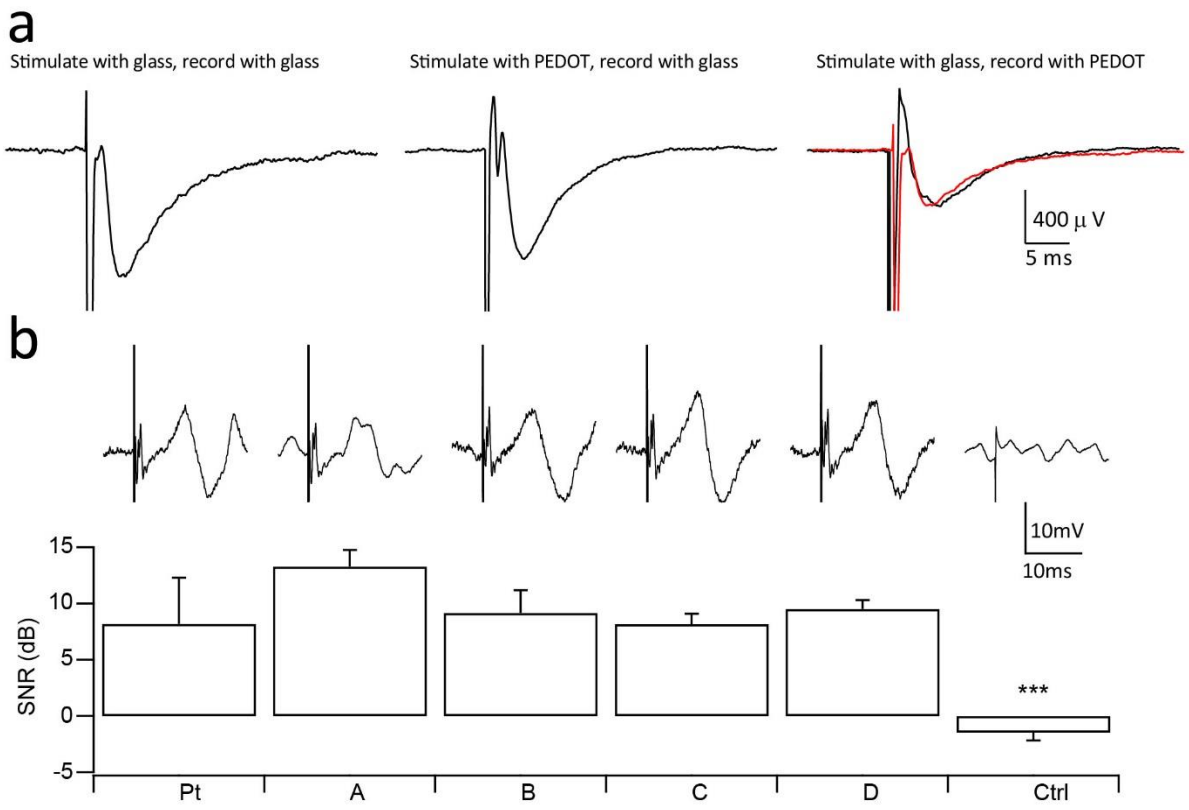

Figure 5. **a)** Stimulating and recording electrical activity in neurons in an acute brain slice (hippocampal region). **b)** Comparison of recording capability on auditory cortex between 3D-PEDOT electrodes. Pt: platinum ball; a variety of 3D-PEDOT electrodes A= Length (100 µm), Width (400 µm), thickness(100 µm); B= L(5,000µm) W(400 µm) t(100 µm); C= L(10,000 µm) W(800 µm) t(100 µm); D= L(10,000 µm) W(1,200 µm) t(100 µm); non-conducting 3D-

PLLA Ctrl.= L(100 µm) W(400 µm) t(100 µm). p <0.0001(****), p = 0.0019(**). Data are mean ± SEM.

Platinum electrodes create scarring due to their relative high modulus compared to the softer neural tissue surrounding it.[5] As a result, when micro movements occur (such as during the heart beat), the miss-match in stiffness means that the electrodes do not deform in synchrony with the neural tissue, and this generates a mechanical stress stimulus on the surrounding cells. The stimulus is sensed through a palette of localized elements including mechanosensitive ion channels, forced unfolding of proteins and the remodeling of focal adhesion sites, which ultimately leads to shear-induced inflammation or encapsulation of the electrode.[47] Therefore, the cellular response to implantation of 3D-PEDOT mats was evaluated in rats at 21 days after surgery. Immunohistochemically stained cross-sectional brain slice images (**Fig.6**) show the infiltration of microglia (ionized calcium binding adaptor molecule 1(Iba1), red staining in **Fig.6a**) in the 3D-PEDOT membrane. The presence of microglia is to be expected as they are the immune guardians of the brain. However, significant activation was not observed. In support of this, there is minimal reactive gliosis, which is indicated by the lack of upregulation of glial fibrillary acidic protein (GFAP, red staining in **Fig.6b**) expression in response to material implantation after 21 days. Importantly, the images also showed neurites within the implanted microfiber electrodes, although this was only modest at this stage. This result is expected since previous studies revealed that neurite ingrowth does not fully emerge until 30 to 60 days *in vivo*.[48-49] In summary, there was little evidence of reactive, stress-induced scarring.

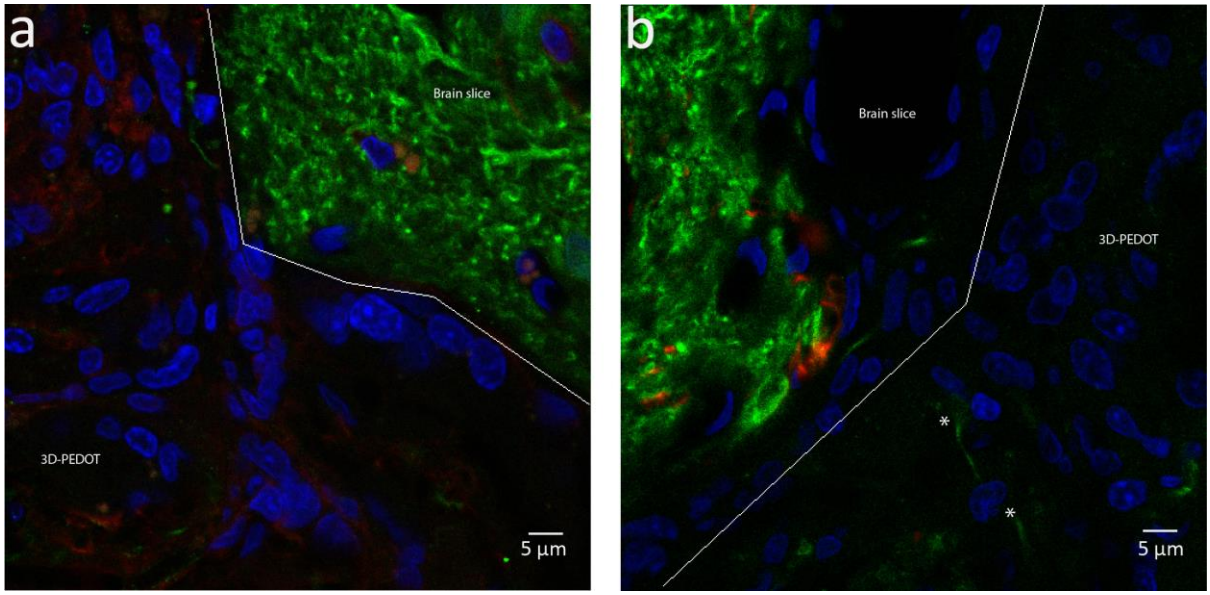

Figure 6. Immunohistochemically stained cross-sectional brain slice images (21 days post implantation) showing neurons, as indicated by βIII-tubulin staining in green, with blue DAPI staining of nuclei; interface is shown by white line. **a)** Activated microglia as indicated by Iba1 staining of cell bodies in red, **b)** Astrocytes as indicated by GFAP staining in red; white stars(*) indicate neurites within the implanted 3D-PEDOT mat.

3. Conclusions

A fibrous conducting 3D organic electrode was successfully developed and these electrodes supported neuronal maturation, diversity and network functioning. Importantly, the 3D electrode was capable of recording from and stimulating electrical activity in neurons *in vitro* and *in situ*. The combination of low noise and high flexibility make 3D-PEDOT-based electrodes ideal for electrocorticography during, for example, the localization of epileptogenic zones. The absence of a glial scar upon implantation *in vivo* and the ability of 3D-PEDOT to conform to the complex topography of the cortical surface would allow better contact between the active recording electrodes and the underlying neural tissue than traditional platinum and silicon based electrode arrays, potentially further improving the effective signal-to-noise ratio. The patterned application of PEDOT to the otherwise non-conductive uncoated PPLA fiber substrate could allow the manufacture of a high density electrode array to improve spatial resolution while maintaining a form factor that is amenable to simple surgical implantation.

4. Experimental Section

Fabrication of electrodes: Our approach first involved the electrospinning of a microfibrous polymeric template. Poly-L-lactic acid PLLA (Sigma) was electrospun with a 2.2.D-300 electrospinner (Yflow) from a 20% wt solution of 3:1 chloroform (Sigma): acetone (Sigma). PLLA granules (0.8g) were dissolved in solvent (4 mL). The solution was mixed thoroughly overnight. Fibers were obtained using a 16 kV voltage with a flow rate of 0.2 mL/hr onto a plate collector at a working distance of 18 cm.

After completing the electrospinning process, the microfiber mats were transferred to a vacuum chamber to remove all traces of solvent, followed by the addition of a conductive PEDOT coating which endowed the microfibers with electroactive properties. The polymeric films and fiber mats were attached to a glass substrate, which served as a rigid carrier during the VPP protocol[26]. The substrate was spin coated with an oxidative solution (40% wt Fe (III) tosylate and 0.023mg/ml pyridine diluted in 1:1 butanol) at 1500 rpm for 30 s. Afterwards, the substrates were exposed to ethylenedioxythiophene (EDOT) monomer vapour at 70˚C for 45 min, resulting in PEDOT coated substrates. Samples are referred as 2D-PEDOT and fiber monolayer PEDOT (FM-PEDOT) for PEDOT coated flat substrates and PLLA monolayered subtrates, respectively. PEDOT coated PLLA fibrous membranes are referred to as 3D-PEDOT.

Characterization of fibrous membranes: The morphology of electrospun fibrous membranes, before and after PEDOT coating, was investigated using scanning electron microscopy (SEM). Samples were adhered to a sample stub using carbon tape. A 1 nm platinum or iridium coating was applied to the sample using a plasma sputter coater. Images were acquired using a 5kV accelerating voltage at a 5mm working distance using an FEI NovaSEM 450 field emission SEM. The electrical properties of the PEDOT coated substrates were studied in terms of sheet resistance (Ω/□) measured using a 4-point probe (Jandel Engineering Ltd) connected to the source meter. The probe is fitted with four spring loaded tungsten carbide needles spaced 870 µm apart. During a measurement sequence the protocol defined by our group was used.[34] Impedance measurements were carried out on a Solartron 1255A Frequency Analyzer at room temperature and at open circuit voltage with a

voltage amplitude of 50 mV. Each sample was cut to a size of 1 x 1 cm. A ~1 mm strip of silver conductive epoxy (Chemtronics) was applied to both front and back sides of the electrode. The samples were annealed for 1 hour at 80 °C to stabilize the conductivity of the silver. Upon cooling, the samples were immersed into 0.1M phosphate buffer solution (PBS, pH=7) for a minimum of 15 minutes to ensure complete pore filling. The samples were attached to a flattened alligator clip for electrical contact to the applied silver strips, then immersed into a two electrode electrochemical setup with 0.1 M PBS as the electrolyte and platinum as the counter electrode. The inter-electrode spacing was ~0.3 cm. Care was taken to ensure that the clips and silver strip were not immersed into the PBS for the measurements. Multiple scans were conducted and duplicate samples analyzed to ensure consistent results. Relative resistance upon flexure was performed according to an established protocol[41] using PEDOT samples with a size of ~2.5 x 0.7 cm^2. At both ends of the long edge silver epoxy (OW Circuitworks) was applied and the exposed ends of 4 cm long electrical leads were embedded within the epoxy. To stabilize the conductivity of the silver epoxy the samples were heated at 80 °C for 20 minutes in air. Resistance measurements were carried out using a conventional voltmeter connected to the electrical leads attached to the PEDOT samples. The samples were manually bent across a surface with a curvature radius of 1 mm.

Hippocampal cell cultures: Primary hippocampal neurons from embryonic day 18 (E18) rats were used for *in vitro* studies. These procedures were approved by the Monash University Animal Ethics Committee and conform to the Australian National Health and Medical Research Council code of practice for the use of animals in research. Pregnant rats (day 18) were deeply anaesthetized using isoflurane, rapidly decapitated using a guillotine and brains were isolated from the pups. Hippocampi were dissected free and single cells were isolated using trypsin (0.25mg/mL) (Sigma-Aldrich). The cells were resuspended in Dulbecco's Modified Eagle's Medium (DMEM) (Gibco) containing 10% fetal calf serum (FCS) and penicillin/streptomycin (100U/mL), and seeded (250,000cells/mL) onto sterilized samples, one per well in a 24-well plate, according to our previous protocol.[37] Two hours later, when cells had adhered to the substrate, Neurobasal A medium (1 ml) containing pen/strep (100u/mL), glutamine (2.5mM) and B27 (2%) (all from Invitrogen) was added to each well. Fifty percent of the medium was replaced every 3 days. The harvested cells consisted of a mixed population of neurons and astrocytes, with a high neuron percentage. A mixed neuron and astrocyte population mimics the natural neuronal environment. All cell culture reagents used were purchased from Invitrogen (Mulgrave, Australia) unless specified below.

Electrophysiology of cultured cells: 3D-PEDOT and glass-coverslips containing cells were transferred to a perfusion bath at room temperature (RT), and continuously superfused with physiological saline solution (PSS) containing (mM): NaCl 137, $NaHCO_3$ 4, NaH_2PO_4 0.3, KCl 5.4, KH_2PO_4 0.44, $MgCl_2$ 0.5, $MgSO_4$ 0.4, glucose 5.6, HEPES 10, $CaCl_2$ 1.5 at pH 7.4. Glass electrodes, 2-5MΩ resistance, were pulled, fire polished and filled with solution containing (mM): KCl 10, $CaCl_2$ 0.05, Mg_2ATP 4, K-Gluconate 130, Na_2-Phosphocreatine 10, EDTA 0.01, EGTA 0.1, HEPES 10, pH 7.2. Electrophysiological activity was recorded using the patch clamp technique in whole-cell mode using an Axopatch 200A series amplifier controlled by pCLAMP v.10 software. Data were digitized at 5–20 kHz and analyzed using Clampfit 10 (Axon Instruments). Current clamp mode was used to record the

resting membrane potential, input capacitance and resistance. Action potentials were evoked using depolarizing current steps. Voltage clamp mode using 10mV depolarizing steps, from a holding potential of -100mV, was used to record voltage gated inward currents. Tetrodotoxin (TTX) was used to interrupt Na^+ currents (Sigma-Aldrich) .[37] The preparations were fixed in paraformaldehyde 4% immediately upon termination of electrophysiology and were later stained immunohistochemically.

Calcium imaging: Primary hippocampal neurons growing on glass coverslips and 3D-PEDOT were loaded with the calcium indicator Fluo-4 AM (1 µM, Invitrogen, CA, USA) in PSS for 15 min at RT. The preparation was then transferred to an organ bath and continuously superfused with PSS at 2 ml/min. All image acquisition experiments carried out at RT in PSS. Fluorescence images were acquired using a confocal microscope (IX71, Olympus) using a 10X objective, passed through a Yokogawa CSU22 Nipkow spinning disc (Yokogawa Australia Pty. Ltd., Macquarie Park New South Wales, Australia) to a high-sensitivity electron-multiplying Andor iXon CCD camera (Andor Technology PLC, Belfast, N. Ireland). Fluorescence images were acquired every 900 ms and pixel intensities were analysed using Andor iQ 1.9 controller software (Andor). Fluorescence responses were corrected for basal fill (F/F_0). Application of PSS containing 50 mM K^+ (isosmotic Na^+ replacement) for 10 s was used to depolarize the cells to threshold for AP induction (HiK-PSS), glutamate [100µM] plus glycine [100µM] (Glu/Gly) for 10 s to replicate transmitter release, and TTX (0.1 µM) to block voltage-gated sodium channels were used to test neuronal activity.

Image analysis of the Ca^{2+} signals was in terms of time dependent changes in mean fluorescence within a user defined area (25 pixel or 16 µm diameter circle) or region of interest (ROI). The LC–Pro plugin for NIH ImageJ software (National Institutes of Health, Bethesda, MD, USA) was used as a validated automated ROI detection algorithm solution to Ca^{2+} signal transient detection. This algorithm identifies sites of dynamic Ca^{+2} change above statistical ($p < 0.05$) noise and analyses ROIs encompassing Ca^{2+} transients in two dimensional time lapse image sequences .[50] Again, upon completion of the functional studies, the preparations were fixed for later immunohistochemical interrogation.

Hippocampal brain slices: Acute hippocampal brain slices from adult rats (8-10 weeks) are commonly used as model neurons in *ex vivo* studies.[46] Acute slice preparation allows stimulating and/or recording from a neural circuit in isolation from the rest of the brain in controlled physiological conditions, whilst maintaining structural connections that are lost in cell cultures or homogenized tissue. Rats were deeply anesthetized with isoflurane and the brains decapitated into ice-cold artificial cerebrospinal fluid (aCSF) containing 206 mM sucrose, 3 mM KCl, 6 mM $MgCl_2$, 0.5 mM $CaCl_2$, 1.25 mM NaH_2PO_4, 25 mM $NaHCO_3$, and 10.6 mM glucose and continuously bubbled with carbogen (95% O_2 and 5% CO_2). Half of the brain was mounted on a vibrating microtome (Integraslice; Campden), and coronal slices (300 µm thick) were cut in sucrose aCSF. The slices were transferred to a chamber filled with gassed aCSF containing 125 mM NaCl, 3 mM KCl, 1 mM $MgCl_2$, 2.5 mM $CaCl_2$, 1.25 mM NaH_2PO_4, 25 mM $NaHCO_3$, and 10.6 mM glucose in a water bath at 35°C. After 30 min, the aCSF containing the slices was placed at RT. After 1 hr, a slice was transferred to a recording chamber mounted on an upright microscope (Leica DMLSF).

Glass electrodes (2-5MΩ resistance) were either filled with conductive solution and

an Ag/AgCl wire (see above) and then backfilled with aCSF, taking care to retain the solution well distal to the tip of the electrode. To test the PEDOT electrodes, small PEDOT mats were inserted into the glass, trimmed at the tip under a dissecting microscope, and then backfilled with a non-conductive epoxy resin **(Figure S6)**. When stimulating, the electrode was placed over the Schaffer collaterals (SC) of the stratum radiatum region of CA2/CA3 border of the hippocampus, whilst recording electrodes were placed into CA1 stratum radiatum. Electrical stimulation of the SC elicits a stimulus artifact, followed almost immediately by a presynaptic population spike, or fiber volley followed by fEPSP.[51] An Axoclamp-2A amplifier was used to record the signals and Clampfit 10 software (Axon Instruments) was used for data acquisition and analysis.

In vivo studies: All experimental procedures involving animals were approved by the Bionics Institute Animal Research Ethics Committee and Monash Animal Ethics Committee in accordance with the Australian Code of Practice for the Care and Use of Animals for Scientific Purposes and with the guidelines laid down by the National Institutes of Health (USA) regarding the care and use of animals for experimental procedures.

Three (n = 3) young adult (2 male, 1 female) guinea pigs (530-550 g) were used to collect data for the experimental studies. Anesthesia was by isoflurane (3% for induction and 1-1.5% for maintenance) with oxygen (0.5 L/kg/min). A heating pad was used to maintain the core body temperature at 37.0 ± 1°C. Respiration rate (40–100 breaths/min) and end-tidal CO_2 (1–3%) were monitored over the duration of the experiment (3-6 h). Animals were placed in a stereotaxic frame (David Kopf instruments) in an electrically shielded room, and a craniotomy was performed to expose the right auditory cortex. A platinum ball or 3D-PEDOT based electrodes were placed on primary auditory cortex (**Figure S.7**). Surface LFPs were captured at a sample rate of 10 kHz using the Cerebus system (Cyberkinetics; Foxborough, Massachusetts) and processed (stimulus triggered average of 10 repetitions, band-pass filtered 10 – 3000Hz) off-line in IgorPro (Wavemetrics; Lake Oswego, Oregon). At the end of the experiment the animals were euthanized with an overdose of pentobarbital (150 mg/kg, intravenous).[52]

Adult (300-350 grams) male rats (n=4) were anaesthetized with 5% isoflurane in O_2, a tracheal cannula was inserted and connected to a ventilator. The animals were maintained with mechanical respiration using 2-3% isoflurane in O_2 throughout the surgery and the head was secured in a stereotactic frame (David Kopf Instruments) as previously described.[53] Following skin incision, a 1x0.8 cm rectangle craniotomy was made on the skull caudal to bregma and left of the midline, with care taken under a neurosurgical microscope to ensure no damage to the dura and brain tissue. Once the dura was exposed, durotomy was conducted to expose a cortical area larger than the size of testing mat, care was taken not damage brain tissue or blood vessels. A 3D-PEDOT mat (2×5×0.1 mm) was placed directly onto the brain tissue. A piece of Gelfoam (Pfzer Australia) was placed directly over the PEDOT mat to cover the entire craniotomy, then a piece of Gelfilm larger than the size of craniotomy was placed over it to protect the brain. The skin was sutured and the animals recovered. Analgesic and fluid were given as part of standard post-operation animal care. Once fully conscious, the animal was returned to the home cage and standard care provided. After three weeks the animals were anaesthetized and the brains perfusion fixed with 4% paraformaldehyde in PBS (PFA). The isolated brains were cryo-protected and sliced in 40 μm sections, which were stored at -80° C for later immunohistochemistry.

Immunohistochemistry: Neurons cultured for various DIV on glass, 2D-PEDOT and FM and fiber mats were studied using electrophysiology and/or calcium imaging and subsequently fixed in 4% PFA and stored briefly at 4°C. These samples and frozen brain slices were processed for immunohistochemical staining of neurons (mouse monoclonal NeuN antibody, Millipore, MAB377, mouse monoclonal β-III tubulin antibody, Thermo Fisher, 2G10, , mouse monoclonal glutamic acid decarboxylase antibody, Abcam, ab261113, all at 1:500 dilution, and rabbit polyclonal calmodulin kinase II antibody, Santa Cruz, sc13082 1:1000 dilution), astrocytes (rabbit polyclonal glial fibrillary acidic protein (GFAP) antibody, Abcam, ab7260 at 1:1000 dilution), and glia (Iba-1, Novachem, #019-19741 at 1:200 dilution). The cells were washed, permeabilized and blocked and incubated in primary antibody overnight at 4°C on a 50 RPM rocker. Next day, the cells were washed with Tween buffer for 4 x 5 min (600 µL/well) before incubation in secondary antibodies (mouse Alexa 488, green (1:1000 dilution) and rabbit Alexa 568, red (1:1000 dilution)) for 1 hr at room temperature. The cells were washed and finally incubated in 4',6-diamidino-2-phenylindole (DAPI) (1µL/5mL PBS) at room temperature for 5 min to stain nuclei. This step was followed by washing with PBS for 3 x 5 mins (600 µL/well) and proceeded with mounting in DAKO. Mounted slides were stored at 4°C. Images were obtained using a Nikon Eclipse confocal microscope, with excitation lasers at 405 nm (blue for DAPI), 488 nm (green for tubulin and NeuN) and 561 nm (red for GFAP) and a 60x or 100x oil-immersion objective.

Acknowledgments

This project was supported by the Australian Research Council Discovery Project DP140100803, awarded to JSF and HCP. The authors acknowledge use of the facilities within the Monash Centre for Electron Microscopy and Monash Micro Imaging.

References

[1] A. B. Schwartz, *Annu Rev Neurosci* **2004**, 27, 487.
[2] K. C. Cheung, *Biomed Microdevices* **2007**, 9, 923.
[3] L. A. Geddes, R. Roeder, *Ann Biomed Eng* **2003**, 31, 879.
[4] R. Biran, D. C. Martin, P. A. Tresco, *Exp Neurol* **2005**, 195, 115.
[5] V. S. Polikov, P. A. Tresco, W. M. Reichert, *J Neurosci Methods* **2005**, 148, 1.
[6] S. P. Lacour, G. Courtine, J. Guck, *Nature Reviews Materials* **2016**, 1, 16063.
[7] J. P. Seymour, D. R. Kipke, *Biomaterials* **2007**, 28, 3594.
[8] R. A. Green, R. T. Hassarati, L. Bouchinet, C. S. Lee, G. L. Cheong, J. F. Yu, C. W. Dodds, G. J. Suaning, L. A. Poole-Warren, N. H. Lovell, *Biomaterials* **2012**, 33, 5875.
[9] P. Fattahi, G. Yang, G. Kim, M. R. Abidian, *Adv Mater* **2014**, 26, 1846.
[10] R. T. Hassarati, J. A. Goding, S. Baek, A. J. Patton, L. A. Poole-Warren, R. A. Green, *Journal of Polymer Science Part B: Polymer Physics* **2014**, 52, 666.
[11] S. P. Lacour, S. Benmerah, E. Tarte, J. FitzGerald, J. Serra, S. McMahon, J. Fawcett, O. Graudejus, Z. Yu, B. Morrison, 3rd, *Med Biol Eng Comput* **2010**, 48, 945.
[12] W. He, G. C. McConnell, R. V. Bellamkonda, *J Neural Eng* **2006**, 3, 316.
[13] Y. Zhong, R. V. Bellamkonda, *J R Soc Interface* **2008**, 5, 957.
[14] M. Gerard, A. Chaubey, B. D. Malhotra, *Biosens Bioelectron* **2002**, 17, 345.
[15] M. Asplund, T. Nyberg, O. Inganäs, *Polymer Chemistry* **2010**, 1, 1374.
[16] R. A. Green, C. M. Williams, N. H. Lovell, L. A. Poole-Warren, *J Mater Sci Mater Med* **2008**, 19, 1625.
[17] K. A. Ludwig, N. B. Langhals, M. D. Joseph, S. M. Richardson-Burns, J. L. Hendricks, D. R. Kipke, *J Neural Eng* **2011**, 8, 014001.
[18] S. C. Luo, E. Mohamed Ali, N. C. Tansil, H. H. Yu, S. Gao, E. A. Kantchev, J. Y. Ying, *Langmuir* **2008**, 24, 8071.
[19] R. A. Green, R. T. Hassarati, J. A. Goding, S. Baek, N. H. Lovell, P. J. Martens, L. A. Poole-Warren, *Macromol Biosci* **2012**, 12, 494.
[20] M. Asplund, H. von Holst, O. Inganas, *Biointerphases* **2008**, 3, 83.
[21] B. Winther-Jensen, M. Forsyth, K. West, J. W. Andreasen, P. Bayley, S. Pas, D. R. MacFarlane, *Polymer* **2008**, 49, 481.
[22] M. Bongo, O. Winther-Jensen, S. Himmelberger, X. Strakosas, M. Ramuz, A. Hama, E. Stavrinidou, G. G. Malliaras, A. Salleo, B. Winther-Jensen, *Journal of Materials Chemistry B* **2013**, 1, 3860.
[23] V. Karagkiozaki, P. Karagiannidis, M. Gioti, P. Kavatzikidou, D. Georgiou, E. Georgaraki, S. Logothetidis, *Biochimica et Biophysica Acta (BBA)-General Subjects* **2013**, 1830, 4294.
[24] L. H. Jimison, A. Hama, X. Strakosas, V. Armel, D. Khodagholy, E. Ismailova, G. G. Malliaras, B. Winther-Jensen, R. M. Owens, *Journal of Materials Chemistry* **2012**, 22, 19498.
[25] S. S. Nair, B. Kolodziejczyk, K. West, T. S. Hansen, S. B. Adeloju, J. S. Forsythe, B. Winther-Jensen, *RSC Advances* **2015**, 5, 7932.
[26] B. Winther-Jensen, K. West, *Macromolecules* **2004**, 37, 4538.
[27] N. A. Kotov, J. O. Winter, I. P. Clements, E. Jan, B. P. Timko, S. Campidelli, S. Pathak, A. Mazzatenta, C. M. Lieber, M. Prato, R. V. Bellamkonda, G. A. Silva, N.

W. S. Kam, F. Patolsky, L. Ballerini, *Advanced Materials* **2009**, 21, 3970.
[28] A. Zhang, C. M. Lieber, *Chem Rev* **2016**, 116, 215.
[29] W. Zhu, C. O'Brien, J. R. O'Brien, L. G. Zhang, *Nanomedicine (Lond)* **2014**, 9, 859.
[30] T. D. Kozai, N. B. Langhals, P. R. Patel, X. Deng, H. Zhang, K. L. Smith, J. Lahann, N. A. Kotov, D. R. Kipke, *Nat Mater* **2012**, 11, 1065.
[31] J. Liu, T. M. Fu, Z. Cheng, G. Hong, T. Zhou, L. Jin, M. Duvvuri, Z. Jiang, P. Kruskal, C. Xie, Z. Suo, Y. Fang, C. M. Lieber, *Nat Nanotechnol* **2015**, 10, 629.
[32] S. H. Lim, H. Q. Mao, *Adv Drug Deliv Rev* **2009**, 61, 1084.
[33] D. R. Nisbet, J. S. Forsythe, W. Shen, D. I. Finkelstein, M. K. Horne, *J Biomater Appl* **2009**, 24, 7.
[34] T. J. Sill, H. A. von Recum, *Biomaterials* **2008**, 29, 1989.
[35] M. R. Abidian, J. M. Corey, D. R. Kipke, D. C. Martin, *Small* **2010**, 6, 421.
[36] M. H. Bolin, K. Svennersten, X. Wang, I. S. Chronakis, A. Richter-Dahlfors, E. W. H. Jager, M. Berggren, *Sensors and Actuators B: Chemical* **2009**, 142, 451.
[37] J. L. Bourke, H. A. Coleman, V. Pham, J. S. Forsythe, H. C. Parkington, *Tissue Eng Part A* **2014**, 20, 1089.
[38] J. F. Rabek, J. Lucki, B. J. Qu, W. F. Shi, *Macromolecules* **1991**, 24, 836.
[39] K. E. Aasmundtveit, E. J. Samuelsen, O. Inganäs, L. A. A. Pettersson, T. Johansson, S. Ferrer, *Synthetic Metals* **2000**, 113, 93.
[40] J. Edberg, D. Iandolo, R. Brooke, X. Liu, C. Musumeci, J. Andreasen, D. T. Simon, D. Evans, I. Engquist, M. Berggren, *Advanced Functional Materials* **2016**, 26, 6950.
[41] F. Paglia, D. Vak, J. van Embden, A. S. R. Chesman, A. Martucci, J. J. Jasieniak, E. Della Gaspera, *ACS Applied Materials & Interfaces* **2015**, 7, 25473.
[42] Y. Kim, N. Spruston, *Hippocampus* **2012**, 22, 693.
[43] S. Oiki, *The Journal of physiology* **2015**, 593, 2553.
[44] J. T. McKenna, C. Yang, S. Franciosi, S. Winston, K. K. Abarr, M. S. Rigby, Y. Yanagawa, R. W. McCarley, R. E. Brown, *J Comp Neurol* **2013**, 521, 1225.
[45] D. Wang, J. Fawcett, *Cell Tissue Res* **2012**, 349, 147.
[46] C. A. Reid, H. A. Coleman, D. I. Finkelstein, M. K. Horne, J. Drago, *Neuropharmacology* **2006**, 51, 587.
[47] S. Mitragotri, J. Lahann, *Nat Mater* **2009**, 8, 15.
[48] D. R. Nisbet, A. E. Rodda, M. K. Horne, J. S. Forsythe, D. I. Finkelstein, *Tissue Engineering Part A* **2010**, 16, 2833.
[49] D. R. Nisbet, A. E. Rodda, M. K. Horne, J. S. Forsythe, D. I. Finkelstein, *Biomaterials* **2009**, 30, 4573.
[50] M. Francis, J. Waldrup, X. Qian, M. S. Taylor, *J Vis Exp* **2014**, DOI: 10.3791/51560e51560.
[51] D. M. Mathis, J. L. Furman, C. M. Norris, *J Vis Exp* **2011**, DOI: 10.3791/23302330.
[52] J. B. Fallon, S. Irving, S. S. Pannu, A. C. Tooker, A. K. Wise, R. K. Shepherd, D. R. Irvine, *J Neurosci Methods* **2016**, 267, 14.
[53] E. K. Brunton, B. Winther-Jensen, C. Wang, E. B. Yan, S. H. Gooie, A. J. Lowery, R. Rajan, *Frontiers in neuroscience* **2015**, 9.

Supporting Information

Neural electrodes based on 3-dimensional organic electroactive microfibers

Jason Marroquin Reyes, Harold A. Coleman, Mary A. Tonta, Kun Zhou, Bjorn Winther-Jensen, James Fallon, Noel W. Duffy, Edwin Yan, Ammar Abdulwahid, Jacek J. Jasieniak, John S. Forsythe, Helena C. Parkington **

*co-corresponding authors

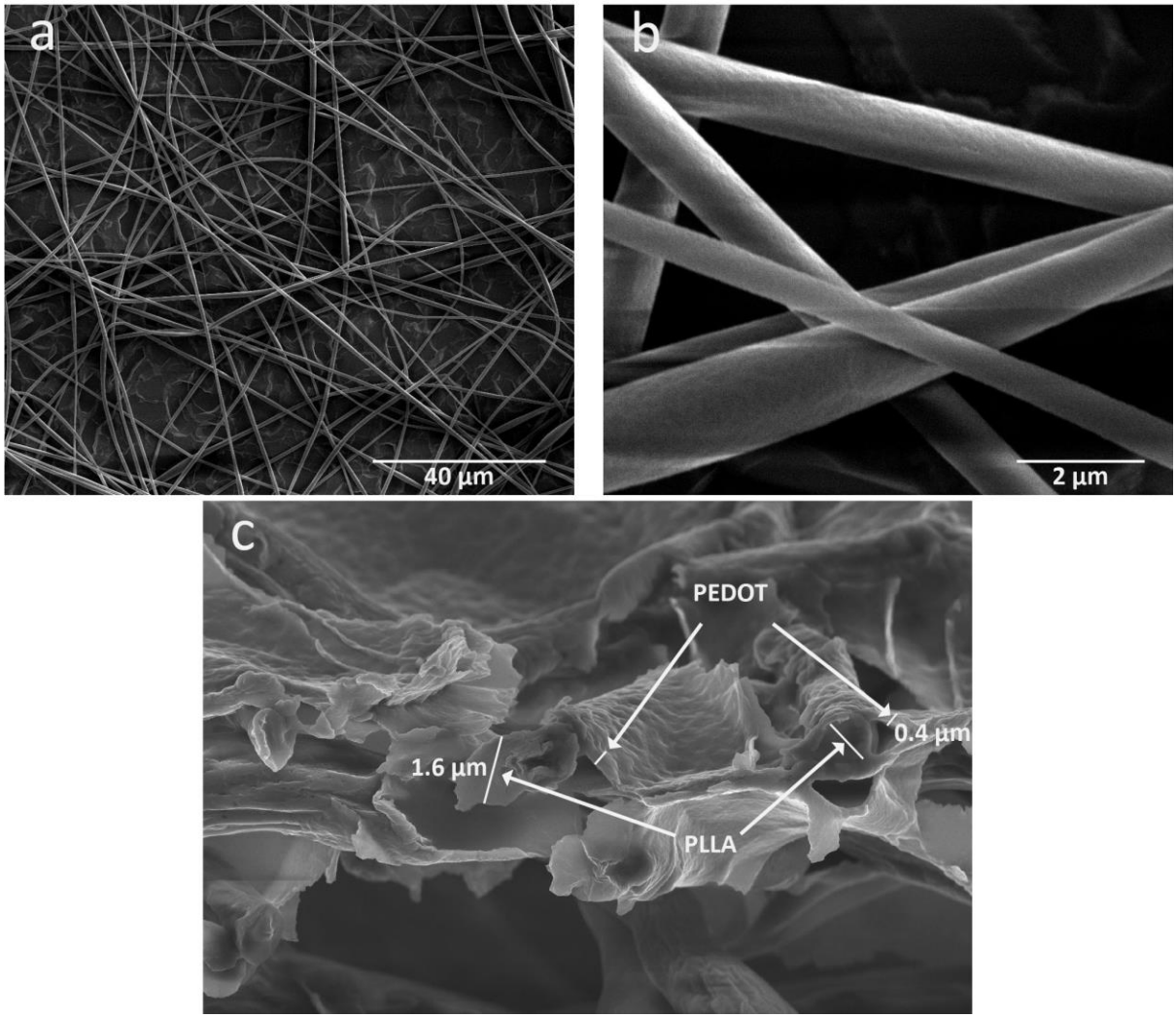

Figure S.1. Scanning electron microscopy (SEM) images of **a)** PLLA fiber monolayer (FM) and **b)** 3D-PLLA fibers **c)** Cross section of PEDOT covered PLLA fibres.

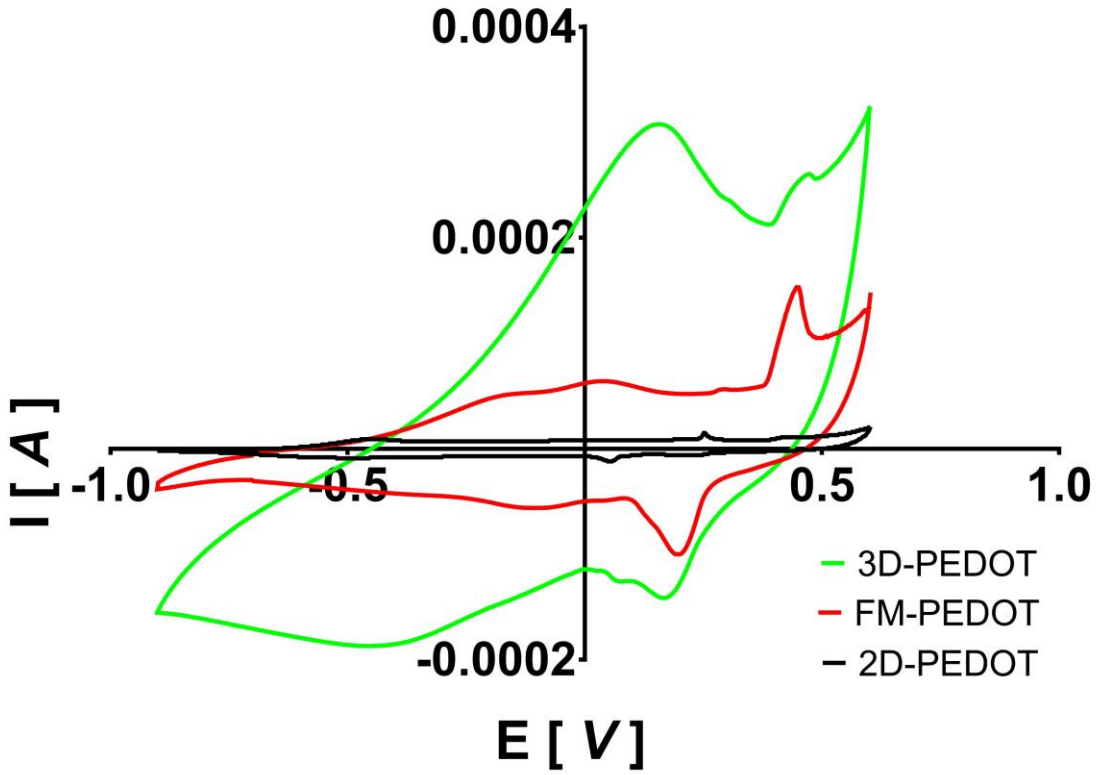

Figure S.2. Cyclic voltammograms of 2D-PEDOT (black), FM-PEDOT (red) and 3D-PEDOT (green) in 0.1M phosphate-buffered saline.

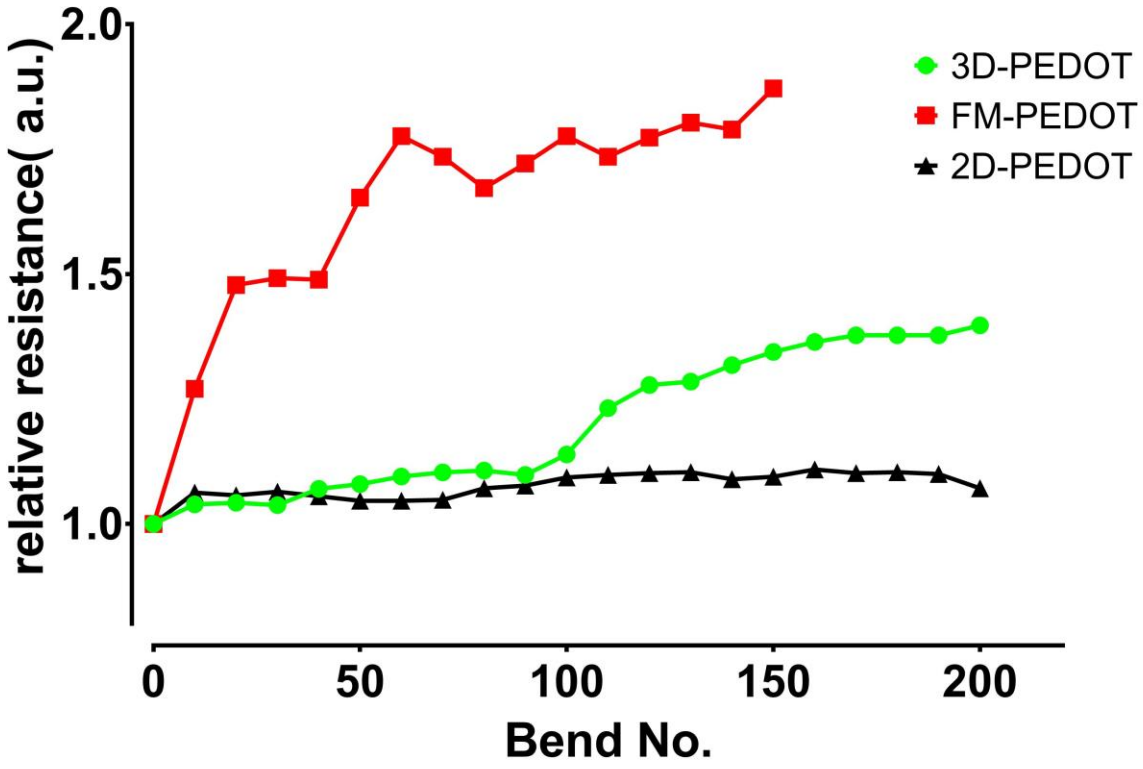

Figure S.3. Variation in Relative Resistance during bending cycles of 2D-PEDOT (black), FM-PEDOT (red) and 3D-PEDOT (green) in air atmosphere.

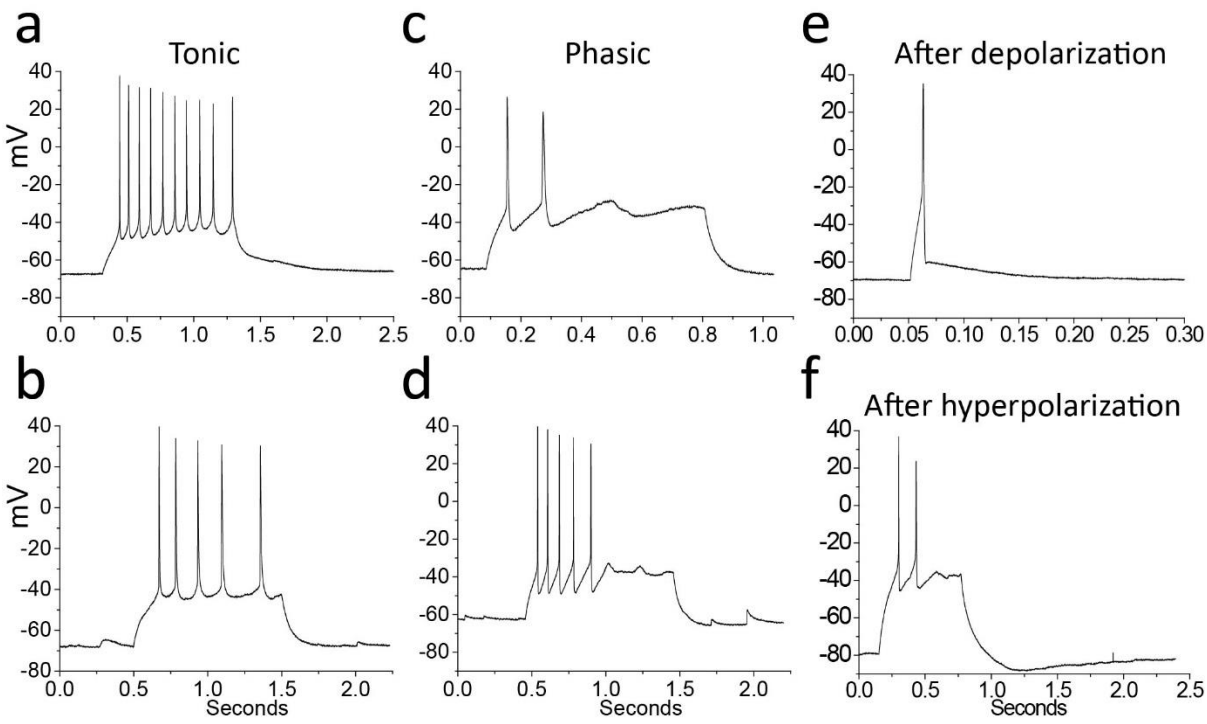

Figure S4. Diversity of cultured neurons (7 DIV) on PEDOT according to their firing patterns in response to depolarizing stimulation. Tonic neurons on **a)** glass and **b)** FM-PEDOT, phasic neurons on **c)** glass and **d)** FM-PEDOT, **e)** a neuron on 2D-PEDOT displaying after-depolarization and **d & f)** neurons (on FM-PEDOT and 2D-PEDOT) displaying after-hyperpolarization.

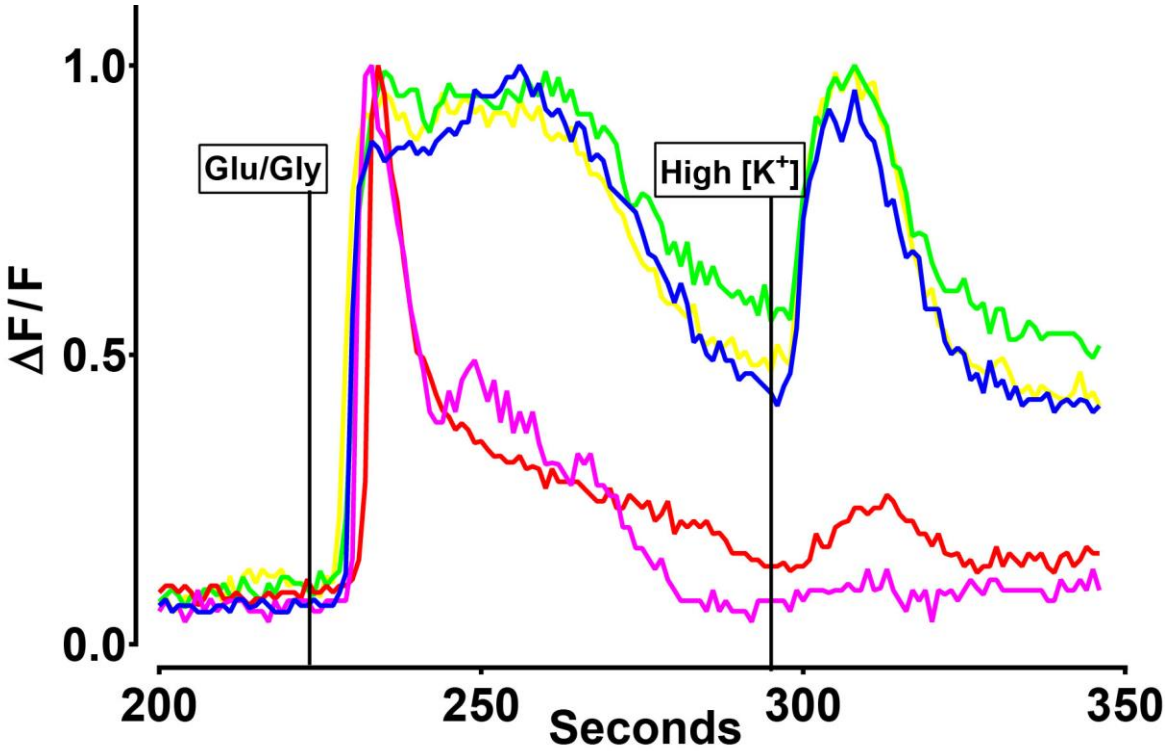

Figure S5. Cytoplasmic calcium levels in cultured hippocampal neurons at 15 DIV.

Summarized fluorescence changes in ROI's calcium from **Figure 3d-f**, on 3D-PEDOT.

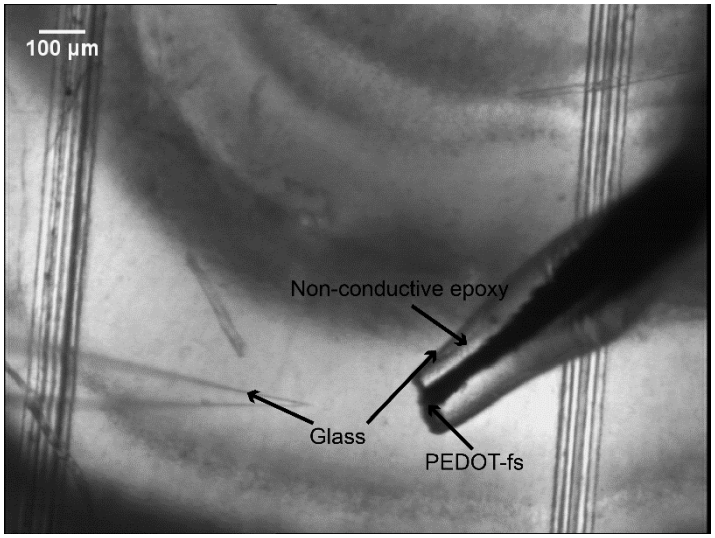

Figure S.6. Bright Field image of 3D-PEDOT electrode used for recording fEPSPs on acute brains slice (hippocampal region).

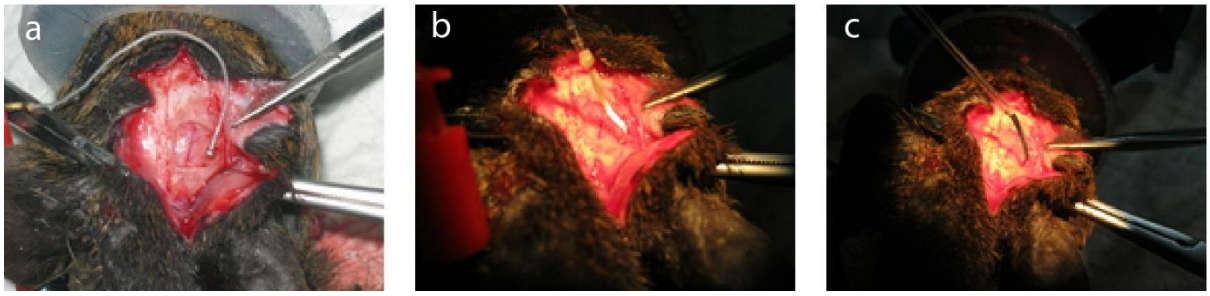

Figure S.7. Electrodes used for surface LFPs recording from guinea pig primary auditory cortex. **a)** Platinum ball **b)** Control **c)** 3D-PEDOT (Electrode B)

Fig S1

Click here to access/download
Supporting Information
S.1.wmf

Fig S2

Click here to access/download

Supporting Information

S.2.tiff

Fig S3

Click here to access/download

Supporting Information

S.3.tiff

Fig S4

Click here to access/download
Supporting Information
S.4.tiff

Fig S5

Click here to access/download

Supporting Information

S.5.tiff

Fig S6

Click here to access/download
Supporting Information
S.6 .tiff

Fig S7

Click here to access/download
Supporting Information
S.7.tiff

Fig 3c left video

Click here to access/download
Supporting Information
Fig.3c(Left) copy.mp4

Fig 3c right video

Click here to access/download
Supporting Information
Fig.3c(right) .mp4

Fig 4(a-f&l) video

Click here to access/download
Supporting Information
Fig.4(a-f&l).mp4

Fig 4k video

Click here to access/download
Supporting Information
Fig4k.mp4

FigS5 video

Click here to access/download

Supporting Information

FigS5.mp4

Figure 1

Figure 2

Figure 3

Figure 4

Figure 5

Figure 6